

# Pattern formation in three–state systems: Towards understanding morphology formation in the presence of evaporation

Emilio N.M. Cirillo<sup>1</sup>, Rainey Lyons<sup>2</sup>, Adrian Muntean<sup>2</sup>, and Stela Andrea Muntean<sup>3</sup>

<sup>1</sup> Dipartimento di Scienze di Base e Applicate per l’Ingegneria (SBAI), Sapienza Università di Roma, Italy,  
`emilio.cirillo@uniroma1.it`

<sup>2</sup> Department of Mathematics and Computer Science, Karlstad University, Sweden  
`rainey.lyons@kau.se`, `adrian.muntean@kau.se`,

<sup>3</sup> Department of Engineering and Physics, Karlstad University, Sweden  
`andrea.muntean@kau.se`

**Abstract.** Inspired by experimental evidence collected when processing thin films from ternary solutions made of two solutes, typically polymers, and one solvent, we computationally study the morphology formation of domains obtained in three-state systems using both a lattice model and a continuum counterpart. The lattice-based approach relies on the Blume–Capel nearest neighbor model with bulk conservative Kawasaki dynamics, whereas as continuum system we consider a coupled system of evolution equations that is derived as hydrodynamic limit when replacing the nearest neighbor interaction in the lattice case by a suitable Kac potential. We explore how the obtained morphology depends on the solvent content in the mixture. In particular, we study how these scenarios change when the solvent is allowed to evaporate.

## 1 Introduction

We are interested in understanding how phase separation takes place in interacting ternary mixtures with one evaporating component. As our work is motivated by applications like building active layers for organic electronics, for instance, like organic solar cells (OSC) [17,10,9,21,23,20,7] and thin polymer composite layers for solution–borne adhesives [11], our focus lies on models describing the time and space evolution of polymer blends in solution where the solvent evaporates. In this paper, we use modeling and simulation tools to address the question: How are morphologies affected by variations in the solvent evaporation rate? Specifically, we make use of a three–state stochastic spin model (referred here as lattice Blume–Capel model, see Section 2) and an associated phase-field type model (a coupled system of nonlinear diffusion-drift equations analyzed in [13]). The results presented here are new and still in a preliminary phase; however, we plan to study the evaporation extensively elsewhere, possibly for the 3D case. Benefiting of our prior experience with alike settings (see, e.g., [3,16,22,14]), we

focus within this framework exclusively on “from-the-top evaporation”, in which evaporation takes place with equal rates on the whole considered domain. Another very interesting case, the so-called “from-the-side evaporation”, in which evaporation takes place only on one of the four sides of the domain, will be treated in detail elsewhere.

As main modeling tool, we use three–state spin lattice systems and study the dependence of the domain growth (like in [5]) on concentration, temperature, and initial composition. Interestingly, we are obtaining values of the growth exponents lower than the typical ones found for the binary models. This fact suggests that the phase separation patterns that can form in such type of systems are complex.

Our interest extends as well to exploring the ability of models based on partial differential equations (PDEs), obtained as continuum limit of three-state spin systems, to describe a similar formation of patterns. Our target PDE system is derived in the literature (see [15]) as the rigorous hydrodynamic limit of a suitably scaled interacting particle system of Blume–Capel-type driven by Kawasaki dynamics. The system we have in mind describes the interaction within a ternary mixture that is the macroscopic counterpart of a mix of two populations of interacting solutes in the presence of a background solvent. We study the qualitative behavior of numerical simulations of finite volume approximations of smooth solutions to our system and their quantitative post-processing in terms of the structure factor indicator. We find many qualitative features (e.g. general shape and approximate coarsening rates) similar to those observed earlier (cf. e.g. [16]) on the stochastic Blume–Capel dynamics with three interacting species.

The paper is organized in the following fashion. We introduce the reader to the topic of three-state stochastic spin models in Section 2 and then illustrate numerically what morphologies can be usually expected as well as what typical effects at the morphology level are visible while varying the evaporation rate. The phase-field model we have in view here is introduced in Section 3. Similarly as in the previous section, we point out our numerical results on typical morphologies obtained now at the continuum level and show effects induced by changing the evaporation rate. We discuss briefly our findings in Section 4.

## 2 The three–state stochastic spin model

Following the ideas firstly introduced in [3] and exploited in [16], we approach the phase separation question for interacting ternary mixtures using the Blume–Capel model, which we describe next for a two-dimensional scenario. Consider  $\mathbb{Z}^2$  embedded in  $\mathbb{R}^2$  and refer to its elements as *sites*. Given two sites  $i, i' \in \mathbb{Z}^2$ , let  $|i - i'|$  be their Euclidean distance. Given  $i \in \mathbb{Z}^2$ , we say that  $i' \in \mathbb{Z}^2$  is a *nearest neighbor* of  $i$  if and only if  $|i - i'| = 1$ . Pairs of neighboring sites will be called *bonds*.

Consider the torus  $\Lambda = \{1, \dots, L\}^2 \subset \mathbb{Z}^2$  and associate each site  $i$  of  $\Lambda$  with a spin variable  $\sigma(i)$  taking values in the *single spin state space*  $\{-1, 0, +1\}$ . We let  $\mathcal{X} = \{-1, 0, +1\}^\Lambda$  be the *configuration* or *state space*.

In the mathematics literature (see e.g., [6,4,5]), the Hamiltonian of the Blume–Capel model is often written as

$$H(\sigma) = J \sum_{\langle i,j \rangle} [\sigma(i) - \sigma(j)]^2 - \lambda \sum_{i \in \Lambda} [\sigma(i)]^2 - h \sum_{i \in \Lambda} \sigma(i), \quad (1)$$

for  $\sigma \in \mathcal{X}$ , where the first sum is extended to the  $2L^2$  bonds with periodic boundary conditions due to the torus topology. The parameters  $J > 0$  and  $\lambda, h \in \mathbb{R}$  are called *coupling constant*, *chemical potential*, and, respectively, *magnetic field*. In the context of spin models a site  $i$  with  $\sigma(i) = \pm 1$  is said to be occupied by a particle with spin  $\pm 1$ , while a site  $i$  with  $\sigma(i) = 0$  is said to be empty. In our polymer interpretation of the model the  $\pm 1$  and  $0$  spins will represent, respectively, polymer and solvent molecules.

We remark that in the physics literature [8,2] the Hamiltonian of the same model is usually written as

$$H(\sigma) = -\bar{J} \sum_{\langle i,j \rangle} \sigma(i)\sigma(j) + D \sum_{i \in \Lambda} [\sigma(i)]^2 - h \sum_{i \in \Lambda} \sigma(i),$$

with  $D$  the *crystal field*. An easy computation yields that the two formulas are equivalent provided  $\bar{J} = 2J$  and  $D = 4J - \lambda$ .

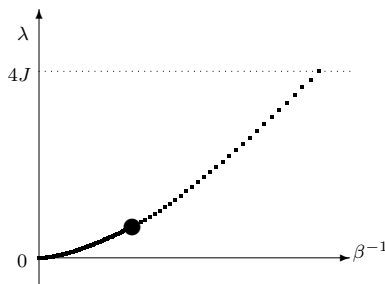


Fig. 1: Schematic representation of the phase diagram in the plane  $\lambda\text{--}\beta^{-1}$ , namely, at  $h = 0$ . Thick solid and thick dotted lines represent, respectively, first and second order phase transition between the low temperature ordered and the high temperature paramagnetic phases. The small disk denotes the tricritical point whose coordinates, see, e.g., [1], are estimated to be  $(0.61, 0.08J)$ . The critical temperature at  $\lambda = 4J$  is 1.69.

The equilibrium state of the model is provided by the usual Gibbs probability measure  $\exp\{-\beta H(\sigma)\} / \sum_{\eta \in \mathcal{X}} \exp\{-\beta H(\eta)\}$ , where  $\beta$  is the inverse of the temperature. The Blume–Capel model phase diagram has been widely studied in the physically relevant region  $D \geq 0$ , which means, with our parametrization,  $\lambda \leq 4J$ . A very rich behavior has been found, see, e.g., [1] and references therein. Indeed, as shown in the schematic phase diagram reported in Fig. 1, at  $h = 0$  the

model exhibits a transition between an ordered and a disordered paramagnetic phase that, depending on the value of  $\lambda$ , is first or second order.

Within this context, we wish to exploit the ability of the model to show three-state pattern formation powering it with a stochastic dynamics which preserves the value of the spins. A natural choice is the reversible, with respect to the Gibbs equilibrium measure, Kawasaki dynamics in which a bond is selected at random with uniform probability throughout the torus and the two spins associated with the two sites of the bond are swapped with probability one if the variation of energy  $\Delta H$  due to the swap is non-positive or with probability  $1 - \exp\{-\beta\Delta H\}$  if  $\Delta H > 0$ .

Indeed, starting from a completely random configuration, with prescribed content of zero, plus, and minus spin, the system, provided the temperature is small enough, will evolve forming domains of constant spin values whose shape and size will strongly depend on the ratio of the spin mixture prescribed *a priori*. We denote, here and in the following, by  $c_0$ ,  $c_1$ , and  $c_{-1} = 1 - (c_0 + c_1)$  the fixed fraction of zeros, pluses, and minuses, respectively.

This coarsening behavior is due to the structure of the Hamiltonian which favors configurations in which spins are surrounded by spins of the same values. The Blume–Capel model has the peculiarity that different interfaces have different energy costs, indeed, according to (1), we have that the minus–plus interface cost  $4J$ , while the minus–zero and minus–plus interface cost is  $J$ . In view of describing morphologies of polymer–polymer–solvent mixtures, the interface costs suggest to interpret the zero spin as the solvent component and the minus and plus spins as the two polymer components.

As mentioned above, we are interested in the morphology formation under evaporation of the solvent component. Then, we have to modify the dynamics of the stochastic Blume–Capel model allowing the zero spins to abandon the lattice. This effect is introduced by drawing at random a site of the lattice at each step of the dynamics and, provided it is a zero, flipping it to minus with probability  $\alpha c_{-1}/(c_{-1} + c_{+1})$  and to plus with probability  $\alpha c_{+1}/(c_{-1} + c_{+1})$ , where  $0 \leq \alpha \leq 1$ . Note that, the drawn zero spin has anyhow the probability  $1 - \alpha$  to be kept at its place in the lattice. Thus, the parameter  $\alpha$  controls the evaporation speed in the sense that the lower is  $\alpha$  the lower is the speed at which the evaporation of the zero component takes place.

## 2.1 Choice of the parameters

As explained above and in Section 1 we are interested in using the stochastic Blume–Capel model to investigate the different morphologies that can be formed due to phase separation. These phenomena will obviously depend strongly on how the parameters appearing in the Hamiltonian will be chosen. But, since we are using the Kawasaki dynamics, the number of minus, zero, and plus spins is conserved during the time evolution, so that the terms in  $\lambda$  and  $h$  in the Hamiltonian are constant and, hence, the two related parameters are not relevant. Thus in the simulations we will always set  $J = 1$  and control the dynamics via the sole parameter  $\beta$ .

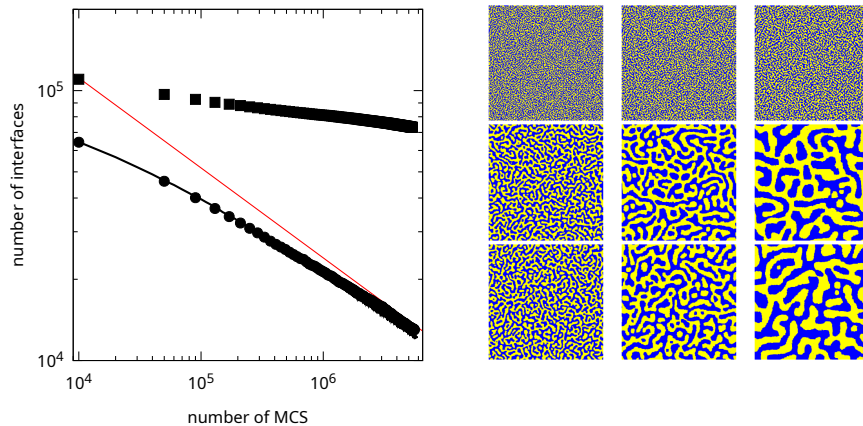


Fig. 2: Number of plus-minus interfaces as function of the number of Monte Carlo Sweeps on the left and system configurations on the right for a simulation on the lattice  $512 \times 512$  with  $J = 1$  and initial uniformly random configuration. For the Blume–Capel model we used  $c_0 = 0$ . **Left:** The black line, the circles, and the squares refer respectively to the Ising system with  $\beta = 1.1$  and the Blume–Capel model with  $\beta = 0.55$  and  $\beta = 1.1$ . The red solid straight line is a reference line with slope  $-1/3$ . **Right:** yellow and blue points represent, respectively, minus and plus spins. From the bottom to the top: Ising  $\beta = 1.1$ , Blume–Capel  $\beta = 0.55$ , and Blume–Capel  $\beta = 1.1$ . From the left to the right MCS =  $10^5$ ,  $10^6$ ,  $5 \times 10^6$ .

In the case in which the zero content  $c_0$  is chosen equal to 0, the system looks like the ferromagnetic Ising model with coupling constant  $J$  with the slightly difference that a plus–minus interfaces costs here  $4J$  with respect to the reference value 0 for the homologous spin bonds, whereas in the Ising model plus–minus interfaces cost  $J$  with respect to the reference value  $-J$  for the homologous spin bonds. Thus, if we denote by  $n'$  and  $n$  the number of interfaces after and before a spin swap on a bond, we have that the change in energy  $\Delta H_{bc}$  and  $\Delta H_i$  respectively for the Blume–Capel and Ising model are

$$\Delta H_{bc} = 4J(n' - n)$$

and

$$\Delta H_i = Jn' - (7 - n')J - [Jn - (7 - n)J] = 2J(n' - n),$$

where we have used that the number of bonds involved in a swap is seven.

Since  $\Delta H_{bc} = 2\Delta H_i$ , we have that if the Ising and the Blume–Capel dynamics are run with the same  $\beta$ , swaps against the energy drift in the Blume–Capel model are highly less probable than in the Ising system. This implies that the Blume–Capel Kawasaki dynamics is highly slower than the corresponding Ising one. We have checked this fact running a simulation on the lattice  $512 \times 512$  for

the Ising model with  $\beta = 1.1$  and the Blume–Capel model with  $\beta = 1.1$  and  $\beta = 0.55$  with zero fraction  $c_0 = 0$ . In Fig. 2, together with the configuration of the system, we have plotted, as a function of the number of Monte Carlo Sweeps (MCS), the number of plus–minus interfaces. It is well known that for the Ising model, in the scaling regime, this number decreases with a power law with exponent  $1/3$ . The number of interfaces has been obtained by measuring the value  $E$  of the Hamiltonian of the time dependent configuration and by computing  $E/4$  in the Blume–Capel simulation with  $c_0 = 0$  and  $(E + 2L^2)/2$  in the Ising simulation.

The picture shows quite neatly the scaling behavior of the Ising model at  $\beta = 1.1$  and of the Blume–Capel model at  $\beta = 0.55$ , while the Blume–Capel model at higher  $\beta$ , after a quick formation of minus and plus structures, appears completely frozen.

However, in the simulations that we will discuss in the following section, we shall always consider cases with  $c_0 \neq 0$  and the presence of zero spin particles will highly speed up the dynamics since the energy cost of zero–plus and zero–minus interfaces is equal to  $J$ . This phenomenon was already noted in [16] and a similar effect was also observed in [18], where a small density of lacunas was added to the Ising model and it was considered a modified Kawasaki dynamics in which only swaps between spins and lacunas were allowed.

In the following, our simulations will be run on the lattice  $512 \times 512$  with parameters  $J = 1$  and  $\beta = 1.1$ .

## 2.2 Morphologies

We discuss, here, the observed morphologies in the regime discussed above in presence of solvent, namely, when the zero content  $c_0$  is not zero. In particular we shall consider the cases  $c_0 = 0.2, 0.4$ , and  $0.8$  reported in Fig. 3. We shall discuss qualitatively the configurations observed during the evolution, but we shall also provide a quantitative characterization of the process by measuring the size of the growing domains by means of the inverse of the first moment of the structure factor. Namely, for any  $(k_x, k_y) \in \{-\pi, -\pi + 2\pi/L, \dots, \pi - 2\pi/L, \pi\}^2$ , we define the structure factor of a 2D configuration as

$$C((k_x, k_y), t) = \frac{1}{L^2} \left| \sum_{(x,y) \in \Lambda} \sigma_t(x, y) e^{i(k_x x + k_y y)} \right|^2. \quad (2)$$

We can then estimate the horizontal and vertical size of the domains by defining

$$R_\alpha(t) = \frac{\sum_{(k_x, k_y)} C((k_x, k_y), t)}{\sum_{(k_x, k_y)} |k_\alpha| C((k_x, k_y), t)}, \quad (3)$$

where  $\alpha \in \{x, y\}$ .

For  $c_0 = 0.2$ , at all times, the minus and plus domains appear to be separated by a layer of zeroes and do not form a bicontinuous structure. It is remarkable

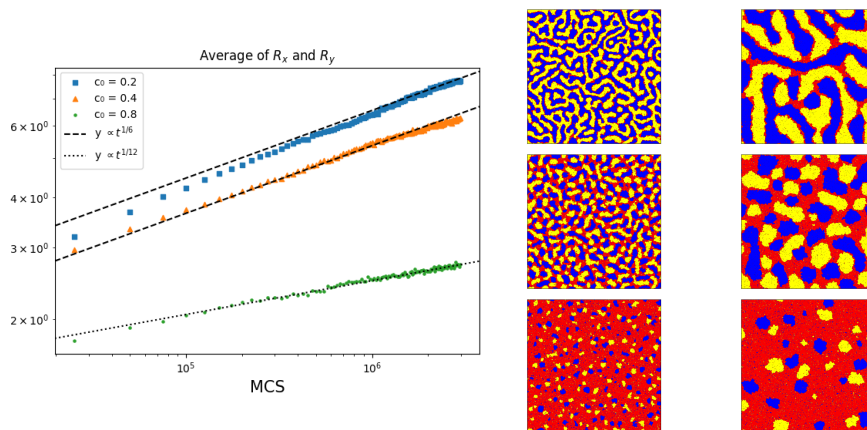


Fig. 3: **Left:** Time evolution of the domain sizes given by the structure factor for the lattice model with reference lines  $y = Ct^p$ . **Right:** Snapshots of the morphologies at early and final time steps (columns) for solvent ratio levels 0.2, 0.4, and 0.8 (rows).

that they have a strongly oblong shape during the whole evolution. This results in a growth exponent smaller than the usual  $1/3$  value typical of the two-state system and found in Section 2.1 in the  $c_0 = 0$  case. This is in agreement with what we found in [16, bottom panel of Fig. 2], where we have shown that the classical exponent  $1/3$  is recovered in the case  $c_0 = 0.1$  in a time interval in which the bicontinuous phase is observed in the lattice, see [16, second row of Fig. 3].

In contrast, in the  $c_0 = 0.8$  case the solvent background is so predominant that the plus and minus domains are small, almost spherical symmetrical balls, growing slowly via a very complicated mechanism: minuses and pluses have to abandon their clusters (which is a highly improbable event), walk through the zero background, and be captured by a larger cluster. This mechanism is so slow that a smaller growth exponent is measured.

The case  $c_0 = 0.4$  seems to be an intermediate situation, indeed, the domains are oblong at initial times, while tend to become spherically symmetric at larger times. Even the growth rate tends to switch from the  $c_0 = 0.2$  to the  $c_0 = 0.8$  behavior.

### 2.3 The effect of evaporation

As explained in Section 2 we consider a modified version of the stochastic model to implement the possibility of the evaporation of the solvent (zero) component. This is realized uniformly on the lattice and is controlled by the parameter  $\alpha$  which tunes the evaporation rate.

In Fig. 4 we report our findings for  $\alpha = 10^{-4}$ ,  $10^{-5}$ , and  $10^{-6}$ . In all the simulations discussed in this section the initial solvent content is  $c_0 = 0.8$ .

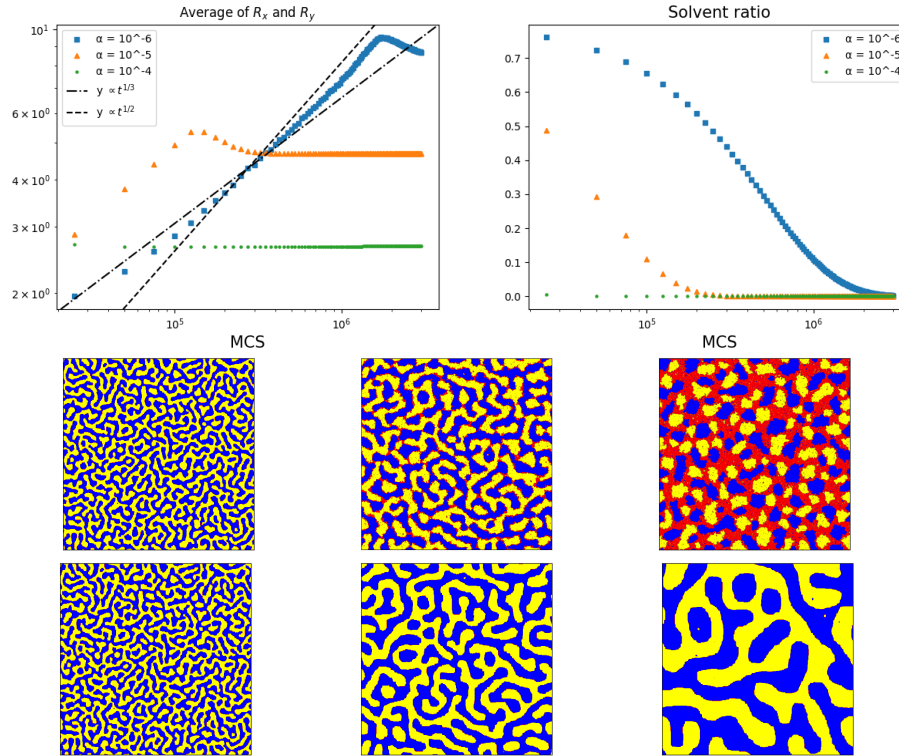


Fig. 4: **Top left:** Time evolution of the domain sizes given by the structure factor for the lattice model with reference lines  $y = Ct^p$ . **Top right:** Evolution of the solvent ratio throughout the simulation. **Bottom:** Snapshots of the morphologies at an early time (top row) and a late time (bottom row) for evaporation probabilities  $\alpha = 10^{-4}$ ,  $10^{-5}$ ,  $10^{-6}$  (columns).

The case  $\alpha = 10^{-4}$  is absolutely trivial, indeed, evaporation is so fast that all the solvent is quickly removed from the lattice so that the system behaves as the stochastic Blume–Capel model with  $c_0 = 0$ . The dynamics, thus, as discussed in Section 2.1, freezes and no coarsening is observed in the time scale that we could simulate.

The cases  $\alpha = 10^{-5}$  and  $10^{-6}$  are, indeed, much more interesting. The initial time configurations are very similar to those that we observed in absence of evaporation at solvent concentration  $c_0 = 0.4$ . Nevertheless, the growth rate seems to be higher, with exponents close to the values  $1/3$  and  $1/2$  which are typical of the two–state systems, respectively, for conserved and non–conserved dynamics. This can be explained since in presence of evaporation, the dynamics is no more locally conserved, indeed spins are directly flipped from zero to plus or



minus when an evaporation event happens. In some sense, the way in which we have introduced evaporation gives to the dynamics a sort of Glauber character.

In perfect agreement with what we observed in Section 2.1 at later times, when the solvent component is fully evaporated, the dynamics freezes. The transition between the coarsening to the frozen regime happens, for  $\alpha = 10^{-5}$  and  $10^{-6}$ , with the appearance of a hump in the domain size plot. This can be related to the fact that the final layer of zeros separating minus and plus disappears and hence direct interfaces are produced.

### 3 The continuum model

The spin lattice model discussed in Section 2 has several nice modelling features, such as its flexibility and the fact that it is easy to be simulated. On the other hand, the way in which we have introduced the evaporation effect is rather brutal and not straightforward. It is then natural to try a different modelling strategy, switching from lattice to continuous space models. This can be realized by considering a continuum limit of the Blume–Capel model. This cannot be done with the nearest–neighbors interaction considered in Section 2, but a new version of the model with a Kac–type long range interaction must be considered.

Following [15] we let  $\gamma$  be a positive real number and consider on  $\mathcal{X}$  the Hamiltonian

$$H_\gamma(\sigma) = \frac{1}{2} \sum_{i \neq j \in \Lambda} J_\gamma(i-j) [\sigma(i) - \sigma(j)]^2 - \lambda \sum_{i \in \Lambda} [\sigma(i)]^2 - h \sum_{x \in \Lambda} \sigma(x), \quad (4)$$

where  $J_\gamma : \mathbb{R}^2 \rightarrow \mathbb{R}$  is a Kac potential function, i.e.,

$$J_\gamma(r) = \gamma^d J(\gamma r) \quad (5)$$

for all  $r \in \mathbb{R}^2$ , where  $J \in C^2(\mathbb{R}^2)$  is such that  $J(r) = J(-r)$  (symmetry),  $\int_{\mathbb{R}^2} J(r) dr = 1$  (normalized to 1),  $J(r) = 0$  if  $|r| > 1$  (supported in the unit ball). Note that  $\gamma^{-1}$  is the range of the interaction. We refer to the monograph [19] for more information on the context.

For the Kac version of the model it is possible to compute exactly the free energy in the so–called mean field limit  $\gamma \rightarrow 0$ . This has been done in [15] following the Lebowitz–Penrose approach introduced in [12]. Studying the mean field free energy it is possible to find a phase diagram which shares some similarities with the one reported in Fig. 1 for the original model. For instance, the transition temperature at  $\lambda = 4$  is 1.701 and there is some evidence (see e.g., [15]) of the existence of a tricritical point along the transition line close to  $\lambda = 0.55$  and  $T = 0.68$ .

From our perspective, the main reason to consider the Kac version of the Blume–Capel model is that, in this framework, it is possible to derive rigorously its continuum limit. Indeed, in [15] the authors obtain the following continuum limit – a system composed of two coupled non-local nonlinear parabolic equations

$$\partial_t m = \nabla \cdot [\nabla m - 2\beta(\phi - m^2)(\nabla J * m)], \quad (t, x) \in (0, T) \times \Omega, \quad (6)$$

$$\partial_t \phi = \nabla \cdot [\nabla \phi - 2\beta m(1 - \phi)(\nabla J * m)] + F(\phi). \quad (7)$$

Here,  $t$  and  $x$  represent the time and space variable.  $m$  represents the average spin density (also called *magnetization*), and  $\phi$  represents the average squared spin density (also called *solute volume concentration*). Additionally,  $\Omega \subset \mathbb{R}^2$  is a cube with spatially periodic boundary conditions (i.e., homeomorphic to the unit torus) and  $T$  is some positive time.

As a simple example, we assume that the evaporation rate is proportional to the solvent volume concentration, i.e.,  $F : \mathbb{R} \rightarrow \mathbb{R}$  defined by  $F(r) = \alpha(1 - r)$ . We prescribe the initial data

$$m(t = 0) = m_0 \text{ and } \phi(t = 0) = \phi_0 \text{ in } \bar{\Omega}. \quad (8)$$

As noted in [15], if we set  $u = (m, \phi)$ , our system can be written for  $F = 0$  as a gradient flow structure given by

$$\partial_t u = \nabla \cdot \left( M \nabla \frac{\delta \mathcal{F}}{\delta \bar{u}} \right). \quad (9)$$

The mobility matrix is

$$M = \beta(1 - \phi) \begin{bmatrix} \phi + \frac{\phi^2 - m^2}{1 - \phi} & m \\ m & \phi \end{bmatrix}$$

and the free energy functional  $\mathcal{F}$  is given by

$$\mathcal{F}(u) = \int_{\Omega} f(\bar{u}) \, dx + \frac{1}{2} \int_{\Omega} \int_{\Omega} J(x - x') [m(x) - m(x')]^2 \, dx' \, dx,$$

where  $f(u) = \phi - m^2 + \beta^{-1} [\frac{1}{2}(\phi + m) \log(\phi + m) + \frac{1}{2}(\phi - m) \log(\phi - m) + (1 - \phi) \log(1 - \phi) - \phi \log(2)]$ . In general, if  $F \neq 0$ , then the gradient flow structure is usually lost. Interestingly, the structure could be regained if one would treat the from-the-side evaporation scenario.

### 3.1 Morphologies

Mimicking the results presented in Section 2.2, we aim to measure the growth of the domains formed by the continuum model and qualitatively compare these dynamics to the lattice model. We make use of the natural continuous analog of the structure factor (2) given by

$$C((k_x, k_y), t) = \frac{1}{|\Omega|} \int_{\Omega} m(t, x, y) e^{i(k_x x + k_y y)} \, dx, \quad (10)$$

for  $(k_x, k_y) \in [-\pi, \pi]^2$  and compute the horizontal and vertical size as

$$R_{\alpha}(t) = \frac{\int_{[-\pi, \pi]^2} C(t, (k_x, k_y)) \, dk_x \, dk_y}{\int_{[-\pi, \pi]^2} |k_{\alpha}| C(t, (k_x, k_y)) \, dk_x \, dk_y}, \quad (11)$$

where  $\alpha \in \{x, y\}$ . We point out that in practice, we simulate the continuum model (6) with a finite volume scheme with a uniform mesh (similar to the one

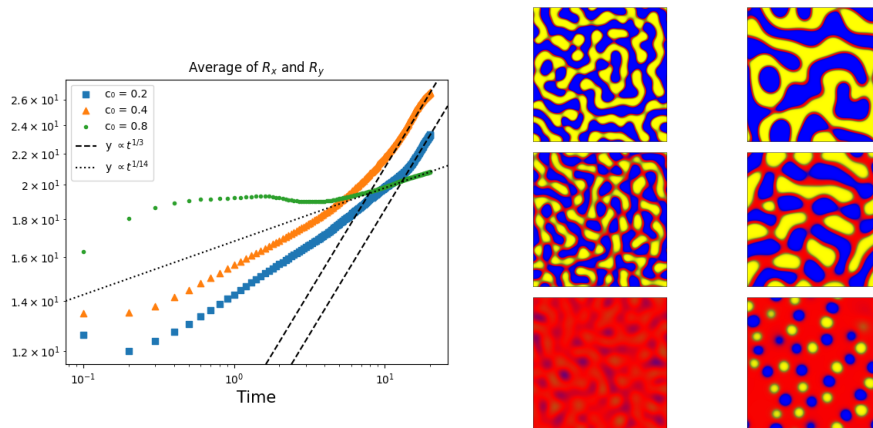


Fig. 5: **Left:** Time evolution of the domain sizes given by the continuous analog of the structure factor. **Right:** Snapshots of the morphologies at early ( $t = 1$ ) and final ( $t = 20$ ) time steps (columns) for solvent ratio levels 0.2, 0.4, and 0.8 (rows).

found in [14]) and these integrals are computed via Riemann sums which closely resemble the discrete counterparts (2) and (3).

In Fig. 5, we plot the evolution of this continuous structure factor over time for the solvent levels  $c_0 = 0.2, 0.4$ , and  $0.8$ . Additionally, we include snapshots of the configurations at an early time ( $t = 1$ ) and the final time of the simulation. Here and throughout the manuscript, we only plot the magnetization field,  $m$ , as the  $\phi$  field is bounded from below by  $|m|$  [13, Theorem 1.1] and therefore is superfluous when the morphologies are well formed (see, however, [14] for configurations of the  $\phi$  field).

Generally, we observe similar qualitative behaviour to that seen in Fig. 3 for the lattice model. Indeed, in the  $c_0 = 0.2$  case, long and strongly connected morphologies are generally observed with a layer of solvent particles separating the  $+1$  and  $-1$  phases. We likewise see similarities with the lattice model in the structure of  $c_0 = 0.4$  and  $c_0 = 0.8$  cases.

Additionally, we see that there are some similarities with regards to the coarsening rates as well. For instance, the case  $c_0 = 0.8$  displays the slowest growth rate due to the phases being isolated in spherical clusters. The  $c_0 = 0.4$  case again acts as a transition regime where the coarsening rate slows down towards the end of the simulation where the phases become more isolated. The difference in the two models appears to be more quantitative as a  $1/3$  power law is achieved during certain time regimes.

### 3.2 The effect of evaporation

Making use of the linear evaporation relation,  $F(\phi) = \alpha(1 - \phi)$ , we can model evaporation in a similar way to that done in Section 2.3.

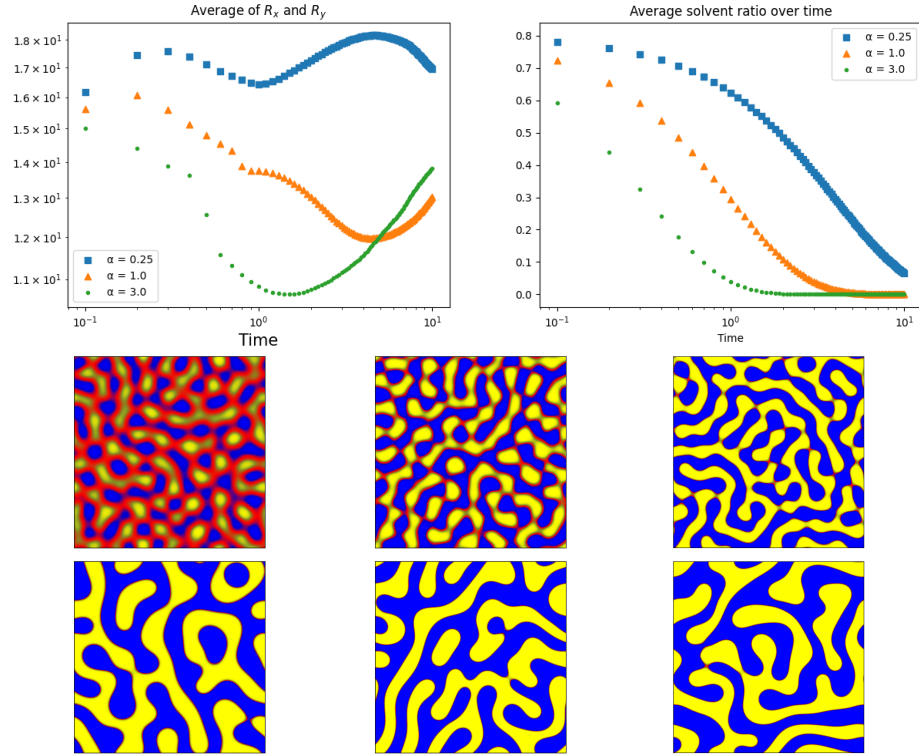


Fig. 6: **Top left:** Time evolution of the domain sizes given by the structure factor for the continuum model. **Top right:** Evolution of the solvent ratio throughout the simulation. **Bottom:** Snapshots of the morphologies at an early time (top row),  $t = 1$ , and the final time (bottom row),  $t = 10$ , for  $F(\phi) = \alpha(1 - \phi)$  and  $\alpha = 0.25, 1, 3$  (columns).

Since the use of indicators (like the structure factor) in continuum models appears to be nonstandard in the literature, we opt to explore measuring the domain sizes in multiple ways. In Fig. 5 and 6, we use the natural continuous analog of the structure factor indicator, however, we see that in the case of evaporation, e.g., Fig. 6, the results are non-intuitive. We explore measuring the domain sizes by first representing the continuum morphologies with a discrete configuration by rounding the phases to the nearest integer, essentially creating a type of sharp interface limit. In Fig. 7, we display an example of this representation.

We can then use the discrete structure factor indicator from Section 2.2. In Fig. 8, we plot the evolution of the structure factor indicator in the absence and presence of evaporation as a function of time on these rounded representations. In both cases, the domains are generally smaller as the rounding process attributes more of the phases to the solvent phase. However, there is a significant difference

in the coarsening rates of the configurations especially in the case of evaporation. Here, instead of the oscillating behavior seen in Fig. 6, we see a much more intuitive size trajectory.

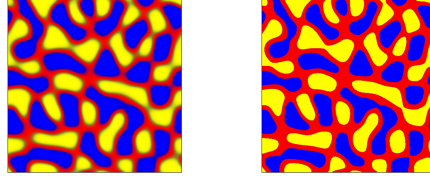


Fig. 7: **Left:** Example of a possible configuration generated by the continuum model (6). **Right:** Rounded representation of the configuration.

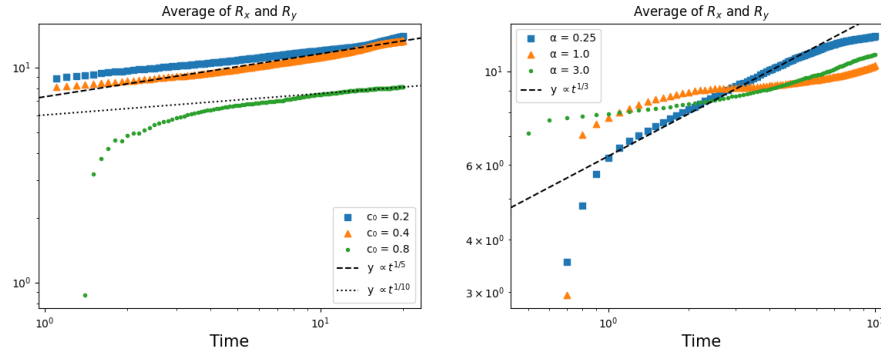


Fig. 8: **Left:** Structure factor calculations for the sharp interface representation of the configurations used in Fig. 5. **Right:** Structure factor calculations for the sharp interface representation of the configurations used in Fig. 6.

## 4 Conclusion

We presented succinctly two conceptually different models that can capture phase separation in ternary mixtures with one evaporating component from two different perspectives – *microscopic* (the three-state stochastic spin model acting on a lattice) and *macroscopic* (the continuum model in terms of partial differential equations). The lattice model is versatile in tuning the interaction parameters and is easier to simulate numerically. On the other hand, modeling evaporation in the lattice model is more tricky, while at the continuum level this

presents no difficulties. Having direct access to a large class of morphologies produced computationally with either of the models, can serve as a starting platform for further investigations, such as a detailed study of the transport of charges through such heterogeneous materials or the study of mechanical properties of such materials.

**Acknowledgments** R.L. and A.M. are grateful to Carl Tryggers Stiftelse for their financial support via the grant CTS 21:1656. S.A.M. would like to acknowledge the funding from the Swedish National Space Agency (Rymdstyrelsen), grant 2021-00137. ENMC thanks the PRIN 2022 project “Mathematical modelling of heterogeneous systems” (code 2022MKB7MM, CUP B53D23009360006). SAM and AM thank the National Academic Infrastructure for Supercomputing in Sweden (NAISS) at the National Supercomputer Centre (NSC) at Linköping University, partially funded by the Swedish Research Council through Grant Agreement Nos. 2022-06725 and 2018-05973.

## References

1. Beale, P.: Finite-scaling study of the two-dimensional Blume-Capel model. *Physical Review B* 33, 1717–1720 (1986)
2. Blume, M.: Theory of the First-Order Magnetic Phase Change in  $\text{UO}_2$ . *Physical Review* 141, 517 (1966)
3. Cirillo, E.N.M., Colangeli, M., Moons, E., Muntean, A., Muntean, S.A., van Stam, J.: A lattice model approach to the morphology formation from ternary mixtures during the evaporation of one component. *Eur. Phys. J. Spec. Top.* 228, 55–68 (2019)
4. Cirillo, E., Jacquier, V., Spitoni, C.: Homogeneous and heterogeneous nucleation in the three-state Blume-Capel model. *Physica D* 461, 134125 (2024)
5. Cirillo, E., Nardi, F., Spitoni, C.: Sum of exit times in a series of two metastable states. *The European Physical Journal Special Topics* 226(10), 2421–2438 (2017)
6. Cirillo, E., Olivieri, E.: Metastability and nucleation for the Blume-Capel model. Different mechanisms of transition. *Journal of Statistical Physics* 83, 473–554 (1996)
7. de Bruijn, R., Michels, J.J., van der Schoot, P.: Transient nucleation driven by solvent evaporation. *J. Chem. Physics* 28(8), 084505 (2024)
8. Fiig, T., Gorman, B., Rikvold, P., Novotny, M.: Numerical transfer-matrix study of a model with competing metastable states. *Physical Review E* 50, 1930–1947 (1994)
9. Huang, Y., Kramer, E.J., Heeger, A.J., Bazan, G.C.: Bulk heterojunction solar cells: Morphology and performance relationships. *Chemical Reviews* 114, 7006–7043 (2014)
10. Kouijzer, S., Michels, J.J., van den Berg, M., Gevaerts, V.S., Turbiez, M., Wienk, M.M., Janssen, R.A.J.: Predicting morphologies of solution processed polymer:fullerene blends. *Journal of the American Chemical Society* 135, 12057–12067 (2013)
11. Kronberg, V.C.E., Muntean, S.A., Kröger, N.H., Muntean, A.: Numerical explorations of solvent borne adhesives: a lattice-based approach to morphology formation. *Modelling and Simulation in Materials Science and Engineering* 31(7), 075005 (2023)

12. Lebowitz, J., Penrose, O.: Rigorous treatment of the van der Waals-Maxwell theory of the liquid-vapor transition. *Journal of Mathematical Physics* 7, 98–113 (1966)
13. Lyons, R., Cirillo, E., Muntean, A.: Phase separation and morphology formation in interacting ternary mixtures under evaporation: Well-posedness and numerical simulation of a non-local evolution system. *Nonlinear Analysis: Real World Applications* 77, 104039 (2024)
14. Lyons, R., Muntean, S.A., Cirillo, E.N.M., Muntean, A.: A continuum model for morphology formation from interacting ternary mixtures: Simulation study of the formation and growth of patterns. *Physica D: Nonlinear Phenomena* 453, 133832 (2023)
15. Marra, R., Mourragui, M.: Phase segregation dynamics for the Blume–Capel model with Kac interaction. *Stochastic Processes and their Applications* 88(1), 79–124 (2000)
16. Muntean, S.A., Kronberg, V.C.E., Colangeli, M., Muntean, A., van Stam, J., Moons, E., Cirillo, E.N.M.: Quantitative analysis of phase formation and growth in ternary mixtures upon evaporation of one component. *Phys. Rev. E* 106, 025306 (2022)
17. Nilsson, S., Bernasik, A., Budkowski, A., Moons, E.: Morphology and phase segregation of spin-casted films of polyfluorene/pcbm blends. *Macromolecules* 40(23), 8291–8301 (2007)
18. Penrose, O., Fratzl, P.: Kinetics of spinodal decomposition in the Ising model with vacancy diffusion. *Phys. Rev. B* 50, 3477 (1994)
19. Presutti, E.: *Scaling Limits in Statistical Mechanics and Microstructures in Continuum Mechanics*. Theoretical and Mathematical Physics, Springer (2008)
20. Ronsin, O.J.J., Harting, J.: Phase-field simulations of the morphology formation in evaporating crystalline multicomponent films. *Advanced Theory and Simulations* 5(10), 2200286 (2022)
21. Schaefer, C., Michels, J.J., van der Schoot, P.: Structuring of thin-film polymer mixtures upon solvent evaporation. *Macromolecules* 49, 6858–6870 (2016)
22. Setta, M., Kronberg, V.C.E., Muntean, S.A., Moons, E., van Stam, J., Cirillo, E.N.M., Colangeli, M., Muntean, A.: A mesoscopic lattice model for morphology formation in ternary mixtures with evaporation. *Communications in Nonlinear Science and Numerical Simulation* 119, 107083 (2023)
23. Wodo, O., Ganapathysubramanian, B.: Modeling morphology evolution during solvent-based fabrication of organic solar cells. *Computational Materials Science* 55, 113–126 (2012)